Workshop on Visualisation in Environmental Sciences (EnvirVis) (2019)
R. Bujack and K. Feige and K. Rink and D. Zeckzer (Editors)

Leveraging Lagrangian Analysis for Discriminating Nutrient Origins

Soumya Dutta[1], Riley X. Brady[2,3], Mathew E. Maltrud[2], Phillip J. Wolfram[2], and Roxana Bujack[1]

[1]Computing, Computational and Statistical Sciences Division, Los Alamos National Laboratory
[2]Fluid Dynamics and Solid Mechanics Theoretical Division, Los Alamos National Laboratory
[3]Department of Atmospheric and Oceanic Sciences and Institute of Arctic and Alpine Research, University of Colorado, Boulder

Abstract

Understanding the origins of nutrients, e.g., nitrate, in ocean water is essential to develop an effective mariculture technique for free-floating macroalgae, which presents a potential solution to provide an alternative source of domestic renewable fuels to help reduce carbon emissions from automobiles. To study this problem, scientists simulate large-scale computational simulations with coupled flow and nutrient information. Since running the simulation multiple times is expensive, the scientists want to have efficient visual-analytic techniques that can analyze and visualize the simulation output quickly to investigate the reasons behind the existence of nitrate in different areas of ocean water. To address these needs, a mixed Lagrangian and Eulerian-based analysis technique is developed that leverages traditional Lagrangian analysis methods and fuses Eulerian information with it to comprehend the origins of nutrients in the water. The proposed method yielded promising results for the application scientists and positive feedback from them demonstrates the efficacy of the technique.

CCS Concepts

• ***Human-centered computing*** → ***Scientific visualization;***

1. Introduction

Development of appropriate feedstock for biofuel production is essential for the development of alternative fuel energy sources [RJSSZ10, WLW*12]. In particular, macroalgae present a plausible solution to reduce carbon emissions from automobiles by providing an alternative source of domestic renewable fuels. Effective mariculture techniques for macroalgae may provide the potential to help close the U.S. transportation carbon budget in the coming years [KPM00, CZL*15]. Understanding the factors contributing to the potential for scalable macroalgae mariculture is non-trivial due to the complexity of ocean flows and mixing, which drives the availability of nutrients for moored and free-floating mariculture techniques. An important challenge for free-floating techniques is the availability of nutrients such as nitrate (NO_3). Hence, studying the sources of NO_3-rich waters is also essential, as ocean eddies may trap macroalgae such as *Sargassum*, and mixing from the NO_3 source to the macroalgae are subject to the complexities of oceanic time-varying currents and turbulence.

In order to study the aforementioned problem, essential flow and nutrient information is simulated using the high-resolution Model for Prediction Across Scales Ocean (MPAS-O) [RPH*13, PJR*15, WRM*15] and its biogeochemistry capability [MDK*01, MLD*13, WBL*14, WEMCS15] within the Energy Exascale Earth System Model (E3SM), formerly known as Accelerated Climate Modeling for Energy (ACME) [PADB*19]. An example output of computed NO_3 is shown in Figure 1, where ocean eddies stir and mix NO_3 that originates from riverine and subsurface locations in the ocean. The output data of the simulation contains velocity and NO_3 information, which can be analyzed and visualized to understand the sources and transport mechanism of nutrient-rich water masses. Note, there are NO_3 source and sink terms, but as demon-

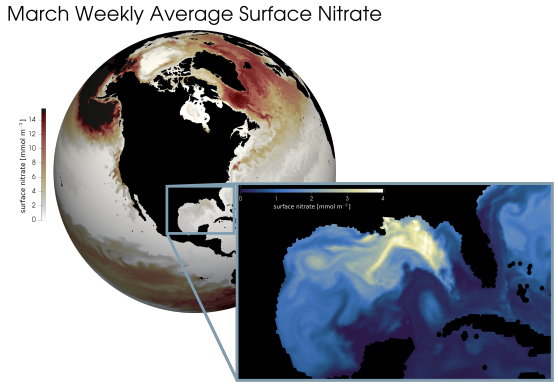

Figure 1: *Globally computed weekly-averaged surface NO_3 (mmol m^{-3}) in March highlighting the Gulf of Mexico (inset).*

DOI: 10.2312/envirvis.20191100

strated in this analysis they are minimal with respect to identifying regions of interest and estimated source locations for NO_3 are reasonable under the assumption that NO_3 is a passive tracer. Since rerunning the simulation at the global scale is significantly expensive, it is necessary to develop an effective *post-hoc* visualization-based workflow such that important information from the simulation output can be extracted efficiently and with minimal effort to further scientist understanding of this problem to guide future experiments in a timely manner.

In this work, a visualization-based workflow is developed which compares and contrasts the evolution of initial nutrient-rich (i.e., regions with high NO_3 concentration) water masses and correlates these regions with high NO_3 concentration in a later time. This helps identify nutrient-rich regions and furthers the exploration of the NO_3 source. The proposed method applies Lagrangian particle advection techniques to track regions where the nutrients would be transported primarily by the surface flow and compares it with the regions of high NO_3 concentration obtained from the scalar NO_3 data defined in Eulerian reference frame. The results show how the surface flow transports the NO_3 into the ocean over time, and furthermore, identify high NO_3-concentrated regions that do not originate from the surface flow. These regions result from potential vertical mixing and upwelling and warrant deeper investigation. Hence, the proposed technique is able to quickly identify source regions for NO_3 that is imperative for understanding the availability of NO_3 for macroalgae mariculture and the suitability of nearby flow conditions for effective seeding, development, and harvesting of *Sargassum* macroalgae.

Since the simulation that produced the data sets use high-resolution ocean models and are run in supercomputers, it is not possible to store all the data to disk. This is primarily because the I/O bottleneck [AJO*14, DCH*17, CPA*10]. The velocity at which data is generated is significantly higher than the speed at which the data can be stored into the permanent disks. Therefore, scientists only typically store temporally averaged and subsampled vector and scalar fields of the surface even though the simulation itself runs on a three-dimensional domain. While investigating the flow patterns of NO_3 and upwelling phenomenon, in this work, this selection of data output seemed a reasonable choice due to the fact that algae can only grow close to the surface where there is sunlight. However, having access to only two-dimensional data imposes two challenges to analysis. First, we cannot use the z-component of the vector field to identify upwelling. Second, there is a strong fluctuation in the instantaneous vector field (see Figure 2) which prevents us from using the second straight-forward approach, namely identifying divergent regions. Since the water is an incompressible fluid, upwelling must result in water spreading away on the surface. This problem has already been identified in [PJMR*19]. Still, we are able to provide the domain expert with meaningful visualization and analysis based on the Lagrangian flow specification. From the results of our analyses, the domain experts got significant insights about the NO_3 transportation mechanism in the ocean water and so the scientists are now considering to store the three-dimensional Lagrangian flow advection information also along with the standard simulation output which will make our analysis more accurate in the future. Therefore, our contributions in this work are as below:

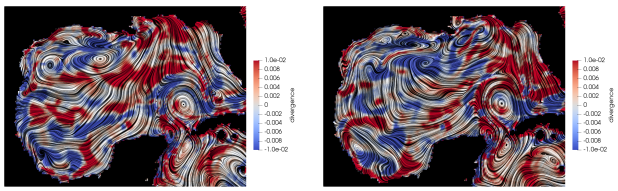

(a) $t = 0.375$ *day.* **(b)** $t = 0.625$ *day.*

Figure 2: *Instantaneous flow behavior for two time steps visualized through line integral convolution color coded by the divergence. Red corresponds to diverging and blue to converging regions.*

1. We present a new mixed Lagrangian and Eulerian-based analysis for identifying the source of NO_3 in the ocean water.
2. We provide an efficient visualization scheme that enables comparative visualization of NO_3-rich regions computed via different methods that helps the experts comprehend the origin of NO_3.
3. We provide the domain experts a workflow to quantitatively analyze the evolution of NO_3 for statistical evaluation.

2. Related Works

The proposed method is related to the general class of analysis that uses tracers to understand ocean model flows [EMR01], but a challenge is that this presumes that the initial tracer location is known *a priori*. Note, that there are connections between Lagrangian and Eulerian approaches for scalar transport, e.g., [WR17], but they use dense Lagrangian trajectories fields that are frequently reset requiring a remapping between Lagrangian fluid control volumes. In another work, to construct a compact representation of large scale simulation data sets, Sauer et al. [SXM17] also proposed a combined Lagrangian and Eulerian data representation by organizing Lagrangian information according to the Eulerian grid into a unit cell-based approach.

The visualization community has developed several analysis techniques that explore ocean simulation data sets for various tasks. For performing eddy analysis and visualization for very high-resolution MPAS-O simulation, Woodring et al. [WPS*16] devised an in situ analysis workflow. Instead of the traditional post-hoc analysis, they performed eddy detection in situ which reduced the bottleneck of disk access time significantly and scaled well to ten-thousand processing elements. To flexibly extract and track eddies in the ocean simulation data sets, Banesh et al. [BSAH17] performed ocean data analysis using an image-based database representation of the simulation output. In another work, Banesh et al. [BWP*18] used statistical change point detection technique for the characterization of eddy behavior in ocean simulation data. Berres et al. [BTP*17] introduced video compression methods for image-based ocean simulation image databases for further reducing the storage size for extreme-scale simulation output. Eddy analysis and visualization of the Agulhas current was done by Raith et al. [RRHS17]. Use of iso-lines was also shown as a popular technique for visualization of ocean simulation data [Sch02]. Streamline and glyph-based visualization was recently used in Open Geosys for an-

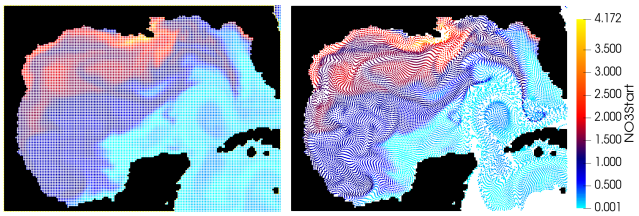

(a) *Particles at $t = 0$ day.* **(b)** *Particles at $t = 6.25$ days.* **(c)**

Figure 3: *Figure 3a shows the starting locations of all the particles, and Figure 3b shows the advected particles at time $t = 6.25$ days. The color of each particle depicts the value of NO_3 at $t = 0$.*

alyzing geothermal energy and groundwater [KBB*12]. Rocha et al. [RSAS17] in their work visually represented the flow direction using sparse streamlet decals to allow for space for simultaneous visualization of salinity and density. Finally, the use of colormaps has also been shown to be effective to visualize ocean flow features [MM98, Ain99].

Recently, Nardini et al. [NBSS17] studied the upwelling process of the Benguela upwelling system using pathline predicates. They derived a 3D volume from pathline density that showed the upwelling process in the ocean. In another work, Nardini et al. [NBP*18] evaluated the accuracy of the pathline predicate based technique. In this work, we study the source of nutrients in the Gulf of Mexico by providing a mixed Lagrangian and Eulerian-based technique. The proposed study helps to determine the origin of NO_3-rich water bodies which can help in developing effective mariculture technique for free-floating macroalgae. For a more comprehensive overview of flow visualization techniques applied in the environmental sciences, we recommend [BM16].

3. Method

In this section, we describe the visual-analytics workflow employed on the simulation data for detecting the source of NO_3 in the ocean water. The primary goal of this work is to be able to compare the source of NO_3 that would come to a region as a result of the surface flow to the regions obtained directly from the NO_3 scalar field, which is defined in the Eulerian frame of reference. Such a comparison can reveal the potential reasons behind the existence of a nutrient-rich region, resulting from either surface advection or vertical mixing and upwelling.

3.1. NO_3 Advection by Lagrangian Analysis

Assuming that the NO_3 can be transported from one region to another due to surface advection, we first identify such potential regions by using the Lagrangian flow advection technique applied to the unsteady velocity field.

A time-varying flow field can be given by both a vector field in its Eulerian representation

$$\mathbb{R}^d \times \mathbb{R} \to \mathbb{R}^d, \quad \vec{x}, t \mapsto \vec{v}(\vec{x}, t) \tag{1}$$

and a flow map in its Lagrangian representation

$$\mathbb{R} \times \mathbb{R} \times \mathbb{R}^d \to \mathbb{R}^d, \quad t \times t_0 \times \vec{x}_0 \mapsto F_{t_0}^t(x_0) \tag{2}$$

satisfying

$$\begin{aligned} F_{t_0}^{t_0}(x_0) &= x_0, \\ F_{t_1}^{t_2}(F_{t_0}^{t_1}(x_0)) &= F_{t_0}^{t_2}(x_0), \end{aligned} \tag{3}$$

The flow map describes how a flow parcel at (x_0, t_0) moves to $F_{t_0}^{t_1}(x_0)$ in the time interval $[t_0, t_1]$. The two representations are related through the initial value problem [Cod12]

$$\dot{F}_{t_0}^t(x_0) = v(x(t), t), \quad F_{t_0}^{t_0}(x_0) = x_0 \tag{4}$$

and inversely through

$$x_0 + \int_{t_0}^{t} v(x(t), t)dt = F_{t_0}^t(x_0). \tag{5}$$

Considering each grid point containing a massless particle at time $t = t_0$, we advect all such particles by integrating over the velocity field for each consecutive time step, as in (5) to compute a Lagrangian trajectory. At each time step t_i ($t_i > t_0$), we record the final position of each particle. Since each particle has a corresponding initial position from where it started advecting at initial time $t = t_0$, we assign the value of NO_3 at the current time t_i for the particle with the value the particle had at $t = t_0$. Therefore, each particle contains the NO_3 value of its initial time step always as it is advected. In particular, if $NO_3 : \mathbb{R}^2 \times \mathbb{R} \to \mathbb{R}$ is the time-dependent scalar field containing the NO_3 distribution, then we get an advected distribution $NO_{3_{t_0}} : \mathbb{R}^2 \times \mathbb{R} \to \mathbb{R}$ starting from t_0 advected to t through

$$NO_{3_{t_0}}(x, t) := NO_3(F_t^{t_0}(x)), \tag{6}$$

where $F_t^{t_0}(x)$ with $t_0 < t$ corresponds to the advection backward in time.

This technique estimates the process of NO_3 advection by surface flow via Lagrangian advection neglecting diffusion processes. In Figure 3, the results of such advection for two selected timesteps have been shown. Figure 3a shows the starting locations of all the particles, and Figure 3b shows their location at $t = 6.25$ days after advection. The particles are colored using the $NO_3(x, 0)$ values they had at $t = 0$.

Given advected particles at each time step, we can effectively identify regions where particles have high NO_3 values. Such a source of NO_3 would be treated as the result of surface flow. To interactively visualize such regions, we first construct a mesh using the particle locations by applying Delaunay triangulation [LS80]. An example of such mesh can be seen in Figure 4a. Next, using surface rendering techniques, we can visualize the surface colored by $NO_{3_{t_0}}$ values as shown in Figure 4b. To identify regions of high $NO_{3_{t_0}}$ concentration, we use isocontour-based visualization as shown in Figure 4b using solid lines on top of the surface rendering. The domain expert can change the $NO_{3_{t_0}}$ isovalue and explore regions of different $NO_{3_{t_0}}$ to identify surface advection.

3.2. Eulerian Frame-based Extraction of NO_3 Regions

Next, in order to identify the source of NO_3 in ocean water, we perform a combined Eulerian and Lagrangian-based comparison of re-

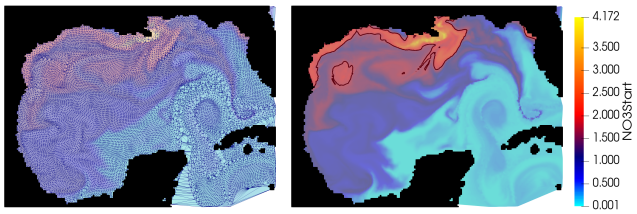

(a) *Triangulated mesh.* **(b)** *Surface visualization.* **(c)**

Figure 4: *Figure 4a shows the triangulated mesh obtained from the particle locations at $t = 6.25$ days, and Figure 4b shows the surface rendering of the Delauney mesh. An isocontour of $NO_{3_{t_0}} = 1.8$ mmol m^{-3} is presented on top showing regions with high $NO_{3_{t_0}}$ values.*

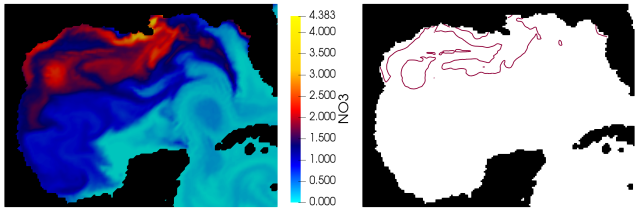

(a) NO_3 *scalar field rendering.* **(b)** **(c)** *Isocontour of NO_3=1.8 mmol m^{-3}.*

Figure 5: *Figure 5a shows the NO_3 scalar field visualization at $t = 6.25$ days, and Figure 5c shows an isocontour of $NO_3 = 1.8$ mmol m^{-3} extracted from the NO_3 scalar field directly.*

gions containing high NO_3 values. In Section 3.1 we discussed how to detect regions containing $NO_{3_{t_0}}$ using Lagrangian-based flow advection. However, the simulation output also contains a scalar field for $NO_3 : \mathbb{R}^2 \times \mathbb{R} \to \mathbb{R}$ defined in the Eulerian reference frame. Therefore, given a specific isovalue of interest at time $t = t_i$, we can visualize the regions that contain NO_3 by plotting isocontours on the NO_3 scalar field directly. The regions enclosed by such isocontours reflect the presence of NO_3 in the surface water at the selected time step. Note that the source of these regions containing NO_3 can be either due to the surface transport or due to vertical mixing of NO_3 and upwelling. In Figure 5a we visualize the NO_3 scalar field at $t = 6.25$ days and in Figure 5c an isocontour of a specific NO_3 value is shown.

3.3. Analysis Workflow and Comparative Visualization Techniques

The analysis workflow is built on top of VTK [SML04], and the processed results are easily importable to ParaView [Aya15] for interactive visualization. A VTK and ParaView-based workflow help us to accelerate the exploration process and the experts can easily adapt this workflow with minimal effort since they are already familiar with ParaView-based workflows.

In order to analyze and visualize the results effectively, we have tested several visualization options. Based on the techniques presented in Section 3.1 and in Section 3.2, for an overview of the

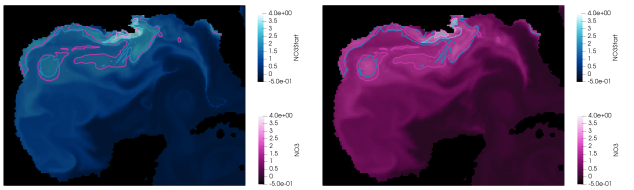

(a) NO_3 *contours with advected NO_3 as context in the background.* **(b)** NO_3 *contours with the Eulerian scalar NO_3 field as context in the background.*

Figure 6: *Comparative visualization of NO_3 contours with NO_3 distributions from different sources are shown in the background as a context.*

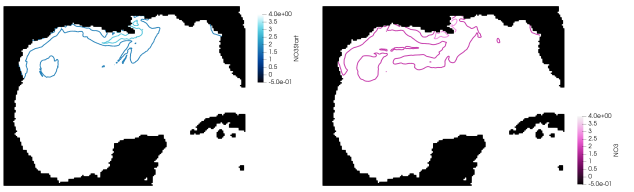

(a) NO_3 *contours of Lagrangian advected $NO_{3_{t_0}}$.* **(b)** NO_3 *contours of the Eulerian scalar NO_3 field.*

Figure 7: *Comparative visualization of NO_3 contours without the context information at $t = 6.25$ days. The simultaneous contour visualization is clean and helps the scientists to visually compare the contour overlapping with minimal effort.*

NO_3 distributions, we can simply use surface rendering as shown in Figure 4b and Figure 5a respectively. However, since the experts are interested in comparing such NO_3 regions obtained from different approaches, we have opted for simultaneous visualization of detected NO_3 regions. For analyzing NO_3 regions that have a particular range of NO_3 values, nested isocontours can be used which can help the experts to isolate regions of interest. Figure 6a shows one example of such isocontour rendering where the red contours show the regions obtained from Eulerian scalar NO_3 data, and the blue contours reflect regions extracted from the Lagrangian analysis. In this figure, the Lagrangian $NO_{3_{t_0}}$ surface is shown at the background as a context to this visualization. Similarly, Figure 6b shows the contours with the Eulerian scalar NO_3 field as the background. In order to make a more cleaner visualization to perform a visual comparison between NO_3 regions, we can just display the isocontours only by turning off the context. Figure 7 shows the results of only contour rendering at $t = 6.25$ days with nested isocontours of NO_3=1.8 and 2.4 mmol m^{-3}. In Figure 8, finally we show the contours of Figure 7 simultaneously on top of each other. By observing these various techniques, the application scientists preferred the simultaneous visualization of contours (Figure 8) over the side-by-side view (Figure 7) as it offered a quick and easy way to perform a visual comparative inspection. During the course of analysis, the expert can interactively turn on/off these different visual representations anytime as required.

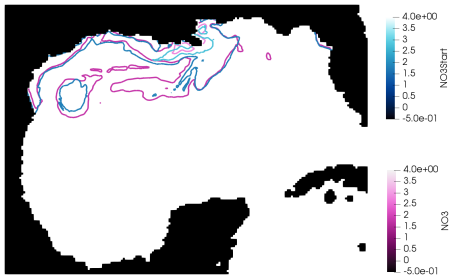

Figure 8: *Simultaneous visualization of NO_3 contours obtained by different techniques for visual comparison.*

Figure 9: *Quantitative analysis of the evolution of the nutrients for statistical evaluation. The areas dominated by advection are light grey, upwelling pink, downwelling blue, and neither black.*

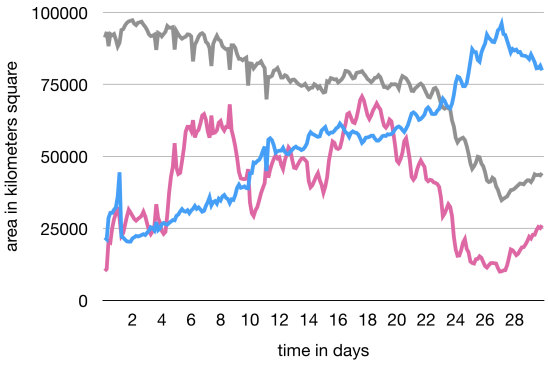

Figure 10: *NO_3 evolution over the course of one month. The areas dominated by advection are light grey, upwelling pink, and downwelling blue.*

3.4. Statistical Analysis

While the domain experts were excited to explore the evolution of NO_3 through the comparative visualization, they expressed that for their work they need more quantitative capabilities; they want to find and quantify patterns of upwelling and downwelling in space and time. Upwelling corresponds to water flowing from depth to the surface and downwelling corresponds to water being subducted from the surface to lower water depths. For example, "Do certain behaviors reoccur during certain times of the day or season and what are the ratios of areas dominated by upwelling to areas dominated by advection?" To the experts, the quantitative metrics, statistics, and longtime correlations are of great value for actual prediction of NO_3 movement.

For this goal, we also perform a quantitative analysis. For a given threshold $c \in \mathbb{R}$ of NO_3 in both scalar fields, we get two binary fields: ${NO_3}^c : \mathbb{R}^2 \times \mathbb{R} \rightarrow [0,1]$ which represents the result obtained by thresholding the Eulerian scalar field using threshold value c (Section 3.2), and ${NO_3}^c_{t_0} : \mathbb{R}^2 \times \mathbb{R} \rightarrow [0,1]$ indicating the thresholded field obtained when the same threshold value c is applied on the scalar field of the surface generated by Lagrangian particle advection technique described in Section 3.1. After the thresholding, we segment the domain into regions with high nutrients based dominantly on advection ${NO_3}^{c^{-1}}(1) \wedge {NO_3}^{c^{-1}}_{t_0}(1)$ (where the segmented regions from Lagrangian and Eulerian fields overlap), on upwelling ${NO_3}^{c^{-1}}(1) \wedge {NO_3}^{c^{-1}}_{t_0}(0)$ (where the segmented regions only come from the Eulerian field), downwelling ${NO_3}^{c^{-1}}(0) \wedge {NO_3}^{c^{-1}}_{t_0}(1)$ (where the segmented regions only come from the Lagrangian field), or neither ${NO_3}^{c^{-1}}(0) \wedge {NO_3}^{c^{-1}}_{t_0}(0)$. Here, $\wedge$ operator denotes the boolean *AND* operation and $(\cdot)$ at the end of each subclause represents whether the subclause is $True = 1$, or $False = 0$. A visualization of this segmentation can be found in Figure 9, but the true benefit is that we can now quantify the behavior based on the area when each of the above criteria is applied. The development of these spatial areas are plotted over the period of one month in Figure 10. As expected, the two scalar fields become less similar over time, which can be observed from the decrease of values for the grey curve. Also, it is observed that upwelling periodically occurs and is variable.

4. Case Study: Mixed Eulerian and Lagrangian-based Comparison of NO_3 Regions

In order to study the source of NO_3 regions in the Gulf of Mexico, we combine the information obtained from the Lagrangian-based analysis (Section 3.1), and Eulerian scalar data-based approach (Section 3.2) for direct comparison purposes. Such a mixed approach of Lagrangian and Eulerian-based analysis was used earlier by Sauer et al. [SXM17] for creating a compact information-rich data representation. The data used in this study is obtained from a simulation, which is a CORE-II interannual forced run (see [PADB*19] for additional configuration details) with fixed atmospheric CO_2 concentration of 360ppm. The simulation underwent a 25-year physics spinup with an additional 20 years of physics and biogeochemistry spinup. We have performed our analysis study on the Gulf of Mexico using a simulation output containing data for one month. The latitude and longitude of this data are 175×130. The complete simulation output contains data for a year and the size is $2.5GB$.

To visualize the regions identified by both the methods, we visualize them using superimposition. In Figure 11, the result is presented. The red contours indicate the regions that are detected from the scalar NO_3 field directly and the isovalues used is 1.8 and 2.4

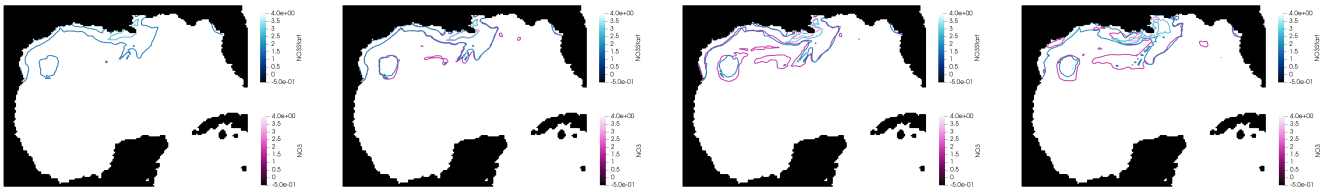

(a) NO_3 *contours at* $t = 0$ *days.* **(b)** NO_3 *contours at* $t = 1.25$ *days.* **(c)** NO_3 *contours at* $t = 5$ *days.* **(d)** NO_3 *contours at* $t = 12.75$ *days.*

Figure 11: *Visualization of superimposed* $NO_{3_{t_0}}$ *contours extracted from Lagrangian advection (blue contours), and Eulerian scalar* NO_3 *data (red contours). Figure 11a shows the contours at initial time* $t = 0$ *days. At this time we start the advection and consequently both the contours overlap each other. Figure 11b shows the result at* $t = 1.25$ *days where we observe regions that have both red and blue contours and are concluded to be the result of surface advection. Figure 11c depicts contours at* $t = 5$ *days. At this time, we see red contours which do not overlap with any blue contours and hence are suspected as the result of vertical mixing and upwelling. Figure 11d shows results from a later time, where upwelling is observed in a different region of the ocean.*

mmol m^{-3}. The blue contours, on the other hand, are the result of the Lagrangian particle-based NO_3 advection presented in Section 3.1 and the same NO_3 isovalues are used here as well. This type of direct superimposition based visualization allows scientists to easily comprehend regions with different properties. In Figure 11a the contours at time $t = 0$ days is presented and at the beginning, they exactly overlap with each other. However, for the future time steps, as we advect particles by integrating the velocity field, the blue NO_3 contours propagate following the particles. We also show the contours obtained from NO_3 scalar field that is defined in the Eulerian frame of reference. In Figure 11b, both the red and blue contours are shown at $t = 1.25$ days.

At $t = 5$ days, (Figure 11c), it is observed that several red contours appear where the blue contours are absent. This observation prompts our scientists to quickly conclude that, since there are no blue contours, such NO_3 regions indicated by red contours are likely formed by upwelling, and not due to the surface advection. This observation coincided with the hypothesis our domain scientists had about the existence of upwelling and further verified that potential NO_3-rich regions can exist in the ocean which are not necessarily formed by surface flow.

Another important observation was made at $t = 5$ days. A red contour was identified that encloses a significantly smaller blue contour. Since the blue contour is quite small, the expert thought that this NO_3 region could be formed by both surface advection and upwelling. The experts further acknowledged that efficient detection of these regions helps them to quickly narrow down regions from the large data sets that need detailed exploration for further understanding.

Figure 11d provides results from a later time of $t = 12.75$ days, where the evidence for the existence of upwelling is found in a different part of the ocean. This observation further strengthens the experts' hypothesis about the existence of upwelling in the simulation data.

5. Discussion

The analysis provides a direct connection between scalar analysis, which is in the Eulerian frame of reference, and Lagrangian analysis, which is in a fluid-following frame of reference. Direct visualization of these mixed quantities are challenging and this visualization presents a a compelling synthesis of both approaches, which to the authors' knowledge is a novel application of Lagrangian particles and contour visualization analysis. The speed at which this computation can occur, even within a contained VTK and ParaView-based workflow indicates the applicability and power of the method to better understand and quantify NO_3 composition within the ocean for NO_3 source assessment, which will be essential for the assessment of *Sargassum* mariculture techniques in free-floating systems that are contained in eddies.

The results from this analysis can be computed quickly and do not require a rerun of the model. Note, however, that the Lagrangian particles computed in this analysis are computed *post-hoc*. Online Lagrangian particle tracking can be employed directly within MPAS-O via the Lagrangian In-situ Global High-performance particle Tracking (LIGHT) capability [WRM*15]. The application scientists had decided not to store Lagrangian particles so far to allow for a higher temporal resolution for Eulerian output. But seeing the power of the Lagrangian analysis, they decided to change the composition of their stored data to allow Lagrangian output. This will facilitate the higher-resolution application of this approach to larger datasets even under temporal sparsity [ACG*14, BJ15].

From the different possible visualizations that we offered the scientists, they preferred the superposition of the contour lines, even though, it looks rather empty. This method provides the clearest visualization using least ink and should therefore also be preferred following the spirit of Tufte [Tuf01]. We decided to keep the semi-transparent color mappings of the two scalar field in the workflow for the application scientists to enable future, more detailed exploration to also satisfy the Shneiderman mantra: overview first, details on demand [Shn03].

6. Conclusion

The economy and efficacy of this method, which uses a mixed Eulerian-Lagrangian computation technique to quickly assess the origins of NO_3 within the Gulf of Mexico, provides a rapid exploration tool that can be used to quickly assess flow field maps with

scalar fields like NO_3. This will allow the origins of waters to be quickly assessed since riverine sources can readily be separated visually from subsurface water sources.

Acknowledgment

We gratefully acknowledge the support of the U.S. Department of Energy through the LANL Laboratory Directed Research Development Program under project number 20190143ER for this work published under LA-UR-19-22455. This research was supported as part of the Energy Exascale Earth System Model (E3SM) project, funded by the U.S. Department of Energy, Office of Science, Office of Biological and Environmental Research as well as the U.S. Department of Energy Advanced Research Projects Agency - Energy (ARPA-E) Macroalgae Research Inspiring Novel Energy Resources (MARINER) program (Funding Opportunity No. DE-FOA-0001726, MARINER Award 17/CJ000/09/01, Pacific Northwest National Laboratory, prime recipient). This research used resources of the Argonne Leadership Computing Facility at Argonne National Laboratory, which is supported by the Office of Science of the U.S. Department of Energy under contract DE-AC02-06CH11357, and resources provided by the Los Alamos National Laboratory Institutional Computing Program, which is supported by the U.S. Department of Energy National Nuclear Security Administration under Contract No. 89233218CNA000001. We also acknowledge the anonymous reviewers for their insightful comments which helped in improving the quality of the paper.

References

[ACG*14] AGRANOVSKY A., CAMP D., GARTH C., E., JOY K., CHILDS H.: Improved post hoc flow analysis via lagrangian representations. In *Large Data Analysis and Visualization (LDAV), 2014 IEEE 4th Symposium on* (Nov 2014), pp. 67–75. doi:10.1109/LDAV.2014.7013206. 6

[Ain99] AINSWORTH E.: Visualization of ocean colour and temperature from multi-spectral imagery captured by the japanese adeos satellite. *Journal of Visualization 2*, 2 (1999), 195–204. 3

[AJO*14] AHRENS J., JOURDAIN S., OLEARY P., PATCHETT J., ROGERS D. H., PETERSEN M.: An image-based approach to extreme scale in situ visualization and analysis. In *SC '14: Proceedings of the International Conference for High Performance Computing, Networking, Storage and Analysis* (Nov 2014), pp. 424–434. doi:10.1109/SC.2014.40. 2

[Aya15] AYACHIT U.: *The ParaView Guide: A Parallel Visualization Application*, 4.3 ed. Kitware Inc., 2015. ISBN 978-1-930934-30-6. URL: http://www.paraview.org/paraview-guide/. 4

[BJ15] BUJACK R., JOY K. I.: Lagrangian Representations of Flow Fields with Parameter Curves. In *Large Data Analysis and Visualization (LDAV), 2015 IEEE 4th Symposium on* (2015), IEEE. 6

[BM16] BUJACK R., MIDDEL A.: Strategic Initiatives for Flow Visualization in Environmental Sciences. In *Workshop on Visualisation in Environmental Sciences (EnvirVis)* (2016), Rink K., Middel A., Zeckzer D., (Eds.), The Eurographics Association, pp. 23–27. doi:10.2312/envirvis.20161103. 3

[BSAH17] BANESH D., SCHOONOVER J., AHRENS J., HAMANN B.: Extracting, visualizing and tracking mesoscale ocean eddies in two-dimensional image sequences using contours and moments. In *Workshop on Visualisation in Environmental Sciences (EnvirVis)* (2017). Workshop on Visualisation in Environmental Sciences (EnvirVis), LA-UR-17-21623. 2

[BTP*17] BERRES A. S., TURTON T. L., PETERSEN M., ROGERS D. H., AHRENS J. P.: Video Compression for Ocean Simulation Image Databases. In *Workshop on Visualisation in Environmental Sciences (EnvirVis)* (2017), Rink K., Middel A., Zeckzer D., Bujack R., (Eds.), The Eurographics Association. doi:10.2312/envirvis.20171104. 2

[BWP*18] BANESH D., WENDELBERGER J., PETERSEN M., AHRENS J., HAMANN B.: Change Point Detection for Ocean Eddy Analysis. In *Workshop on Visualisation in Environmental Sciences (EnvirVis)* (2018), Rink K., Zeckzer D., Bujack R., Jänicke S., (Eds.), The Eurographics Association. doi:10.2312/envirvis.20181134. 2

[Cod12] CODDINGTON E. A.: *An introduction to ordinary differential equations*. Courier Corporation, 2012. 3

[CPA*10] CHILDS H., PUGMIRE D., AHERN S., WHITLOCK B., HOWISON M., PRABHAT, WEBER G., BETHEL E. W.: Extreme Scaling of Production Visualization Software on Diverse Architectures. *IEEE Computer Graphics and Applications (CG&A) 30*, 3 (May/June 2010), 22–31. 2

[CZL*15] CHEN H., ZHOU D., LUO G., ZHANG S., CHEN J.: Macroalgae for biofuels production: progress and perspectives. *Renewable and Sustainable Energy Reviews 47* (2015), 427–437. 1

[DCH*17] DUTTA S., CHEN C. M., HEINLEIN G., SHEN H. W., CHEN J. P.: In situ distribution guided analysis and visualization of transonic jet engine simulations. *IEEE Transactions on Visualization and Computer Graphics 23*, 1 (Jan 2017), 811–820. 2

[EMR01] ENGLAND M. H., MAIER-REIMER E.: Using chemical tracers to assess ocean models. *Reviews of Geophysics 39*, 1 (2001), 29–70. 2

[KBB*12] KOLDITZ O., BAUER S., BILKE L., BÖTTCHER N., DELFS J.-O., FISCHER T., GÖRKE U. J., KALBACHER T., KOSAKOWSKI G., MCDERMOTT C., ET AL.: Opengeosys: an open-source initiative for numerical simulation of thermo-hydro-mechanical/chemical (thm/c) processes in porous media. *Environmental Earth Sciences 67*, 2 (2012), 589–599. 3

[KPM00] KHESHGI H. S., PRINCE R. C., MARLAND G.: The potential of biomass fuels in the context of global climate change: focus on transportation fuels. *Annual review of energy and the environment 25*, 1 (2000), 199–244. 1

[LS80] LEE D.-T., SCHACHTER B. J.: Two algorithms for constructing a delaunay triangulation. *International Journal of Computer & Information Sciences 9*, 3 (1980), 219–242. 3

[MDK*01] MOORE J. K., DONEY S. C., KLEYPAS J. A., GLOVER D. M., FUNG I. Y.: An intermediate complexity marine ecosystem model for the global domain. *Deep Sea Research Part II: Topical Studies in Oceanography 49*, 1-3 (2001), 403–462. 1

[MLD*13] MOORE J. K., LINDSAY K., DONEY S. C., LONG M. C., MISUMI K.: Marine ecosystem dynamics and biogeochemical cycling in the community earth system model [cesm1 (bgc)]: Comparison of the 1990s with the 2090s under the rcp4. 5 and rcp8. 5 scenarios. *Journal of Climate 26*, 23 (2013), 9291–9312. 1

[MM98] MCPHERSON A., MALTRUD M.: Poptex: Interactive ocean model visualization using texture mapping hardware. In *Proceedings of the conference on Visualization'98* (1998), IEEE Computer Society Press, pp. 471–474. 3

[NBP*18] NARDINI P., BÖTTINGER M., POGRZEBA H., SIEGFRIED L., SCHMIDT M., SCHEUERMANN G.: Numerical evaluation of pathline predicatesof the benguela upwelling system. In *Leipzig Symposium on Visualization in Applications (LEVIA)* (2018). 3

[NBSS17] NARDINI P., BÖTTINGER M., SCHEUERMANN G., SCHMIDT M.: Visual study of the benguela upwelling system using pathline predicates. In *EnvirVis17: Workshop on Visualisation in Environmental Sciences* (2017), Eurographics Association. 3

[PADB*19] PETERSEN M. R., ASAY-DAVIS X. S., BERRES A. S., CHEN Q., FEIGE N., HOFFMAN M. J., JACOBSEN D. W., JONES P. W., MALTRUD M. E., PRICE S. F., RINGLER T. D., STRELETZ

G. J., TURNER A. K., VAN ROEKEL L. P., VENEZIANI M., WOLFE J. D., WOLFRAM P. J., WOODRING J. L.: An evaluation of the ocean and sea ice climate of E3SM using MPAS and interannual CORE-II forcing. *Journal of Advances in Modeling Earth Systems* (2019). doi:https://doi.org/10.1029/2018MS001373. 1, 5

[PJMR*19] PHILLIP J. W., MATHEW M., RILEY B., STEVEN B., ZHAOQING Y., TAIPING W.: Multi-resolution, multi-scale modeling of ocean biogeochemistry for scalable macroalgae production, 3 2019. URL: http://permalink.lanl.gov/object/tr?what=info:lanl-repo/lareport/LA-UR-19-22011. 2

[PJR*15] PETERSEN M. R., JACOBSEN D. W., RINGLER T. D., HECHT M. W., MALTRUD M. E.: Evaluation of the arbitrary lagrangian–eulerian vertical coordinate method in the mpas-ocean model. *Ocean Modelling 86* (2015), 93–113. 1

[RJSSZ10] ROESIJADI G., JONES S. B., SNOWDEN-SWAN L. J., ZHU Y.: *Macroalgae as a biomass feedstock: a preliminary analysis*. Tech. rep., Pacific Northwest National Lab.(PNNL), Richland, WA (United States), 2010. 1

[RPH*13] RINGLER T., PETERSEN M., HIGDON R. L., JACOBSEN D., JONES P. W., MALTRUD M.: A multi-resolution approach to global ocean modeling. *Ocean Modelling 69* (2013), 211–232. 1

[RRHS17] RAITH F., RÖBER N., HAAK H., SCHEUERMANN G.: Visual Eddy Analysis of the Agulhas Current. In *Workshop on Visualisation in Environmental Sciences (EnvirVis)* (2017), Rink K., Middel A., Zeckzer D., Bujack R., (Eds.), The Eurographics Association. doi:10.2312/envirvis.20171100. 2

[RSAS17] ROCHA A., SILVA J. D., ALIM U., SOUSA M. C.: Multivariate visualization of oceanography data using decals. In *Workshop on Visualisation in Environmental Sciences (EnvirVis)* (2017). 3

[Sch02] SCHLITZER R.: Interactive analysis and visualization of geoscience data with ocean data view. *Computers & geosciences 28*, 10 (2002), 1211–1218. 2

[Shn03] SHNEIDERMAN B.: The eyes have it: A task by data type taxonomy for information visualizations. In *The Craft of Information Visualization*. Elsevier, 2003, pp. 364–371. 6

[SML04] SCHROEDER W., MARTIN K., LORENSEN B.: *The Visualization Toolkit: An Object Oriented Approach to 3D Graphics*, fourth ed. Kitware Inc., 2004. ISBN 1-930934-19-X. 4

[SXM17] SAUER F., XIE J., MA K.: A combined eulerian-lagrangian data representation for large-scale applications. *IEEE Transactions on Visualization and Computer Graphics 23*, 10 (Oct 2017), 2248–2261. doi:10.1109/TVCG.2016.2620975. 2, 5

[Tuf01] TUFTE E. R.: *The visual display of quantitative information*, vol. 2. Graphics press Cheshire, CT, 2001. 6

[WBL*14] WANG S., BAILEY D., LINDSAY K., MOORE K., HOLLAND M.: Impacts of sea ice on the marine iron cycle and phytoplankton productivity. *Biogeosciences Discussions 11* (2014), 2383–2418. 1

[WEMCS15] WANG S., ELLIOTT S., MALTRUD M., CAMERON-SMITH P.: Influence of explicit phaeocystis parameterizations on the global distribution of marine dimethyl sulfide. *Journal of Geophysical Research: Biogeosciences 120*, 11 (2015), 2158–2177. 1

[WLW*12] WARGACKI A. J., LEONARD E., WIN M. N., REGITSKY D. D., SANTOS C. N. S., KIM P. B., COOPER S. R., RAISNER R. M., HERMAN A., SIVITZ A. B., ET AL.: An engineered microbial platform for direct biofuel production from brown macroalgae. *Science 335*, 6066 (2012), 308–313. 1

[WPS*16] WOODRING J., PETERSEN M., SCHMEIBER A., PATCHETT J., AHRENS J., HAGEN H.: In situ eddy analysis in a high-resolution ocean climate model. *IEEE Transactions on Visualization and Computer Graphics 22*, 1 (Jan 2016), 857–866. doi:10.1109/TVCG.2015.2467411. 2

[WR17] WOLFRAM P. J., RINGLER T. D.: Computing eddy-driven effective diffusivity using lagrangian particles. *Ocean Modelling 118* (2017), 94–106. 2

[WRM*15] WOLFRAM P., RINGLER T., MALTRUD M., JACOBSEN D. W., PETERSEN M.: Diagnosing isopycnal diffusivity in an eddying, idealized mid-latitude ocean basin via Lagrangian In-situ, Global, High-performance particle Tracking (LIGHT). *Journal of Physical Oceanography 45*, 8 (2015), 2114–2133. 1, 6